New Journal of Physics
The open-access journal for physics

# Study of neutrino interactions with the electronic detectors of the OPERA experiment

N Agafonova[1], A Aleksandrov[2], O Altinok[3], A Anokhina[4], S Aoki[5], A Ariga[6], T Ariga[6], D Autiero[7], A Badertscher[8], A Bagulya[9], A Bendhahbi[10], A Bertolin[11,39], C Bozza[12], T Brugière[7], R Brugnera[11,13], F Brunet[14], G Brunetti[7,15,16], S Buontempo[2], A Cazes[7], L Chaussard[7], M Chernyavskiy[9], V Chiarella[17], A Chukanov[18], N D'Ambrosio[19], F Dal Corso[11], G De Lellis[2,20], P del Amo Sanchez[14], Y Déclais[7], M De Serio[21], F Di Capua[2], A Di Crescenzo[2,20], D Di Ferdinando[16], N Di Marco[22,40], S Dmitrievski[18], M Dracos[23], D Duchesneau[14], S Dusini[11], T Dzhatdoev[4], J Ebert[24], O Egorov[25], R Enikeev[1], A Ereditato[6], L S Esposito[8], J Favier[14], T Ferber[24], R A Fini[21], D Frekers[26], T Fukuda[27], A Garfagnini[11,13], G Giacomelli[15,16], M Giorgini[15,16,41], C Göllnitz[24], J Goldberg[28], D Golubkov[25], L Goncharova[9], Y Gornushkin[18], G Grella[12], F Grianti[17,29], A M Guler[3], C Gustavino[19,42], C Hagner[24], K Hamada[27], T Hara[5], M Hierholzer[24], A Hollnagel[24], K Hoshino[27], M Ieva[21], H Ishida[30], K Jakovcic[31], C Jollet[23,47], F Juget[6], M Kamiscioglu[3], K Kazuyama[27], S H Kim[32,43], M Kimura[30], N Kitagawa[27], B Klicek[31], J Knuesel[6], K Kodama[33], M Komatsu[27], U Kose[11,13], I Kreslo[6], H Kubota[27], C Lazzaro[8], J Lenkeit[24], I Lippi[11], A Ljubicic[31], A Longhin[11,13,44], P Loverre[34], G Lutter[6], A Malgin[1], G Mandrioli[16], K Mannai[10], J Marteau[7], T Matsuo[30], V Matveev[1], N Mauri[15,16,43], E Medinaceli[16], F Meisel[6], A Meregaglia[23,47], P Migliozzi[2], S Mikado[30], S Miyamoto[27], P Monacelli[22], K Morishima[27], U Moser[6], M T Muciaccia[21,35], N Naganawa[27], T Naka[27], M Nakamura[27], T Nakano[27], D Naumov[18], V Nikitina[4], K Niwa[27], Y Nonoyama[27], S Ogawa[30], N Okateva[9], A Olchevskiy[18], M Paniccia[17], A Paoloni[17], B D Park[32,45], I G Park[32], A Pastore[21,35], L Patrizii[16], E Pennacchio[7], H Pessard[14], K Pretzl[6], V Pilipenko[26], C Pistillo[6], N Polukhina[9], M Pozzato[15,16], F Pupilli[22], R Rescigno[12], T Roganova[4], H Rokujo[5], G Romano[12], G Rosa[34],


1367-2630/11/053051+22$33.00

**I Rostovtseva[25], A Rubbia[8], A Russo[2], V Ryasny[1], O Ryazhskaya[1], O Sato[27], Y Sato[36], A Schembri[19], W Schmidt-Parzefall[24], H Schroeder[37], L Scotto Lavina[2,20,46], A Sheshukov[18], H Shibuya[30], G Shoziyeov[4], S Simone[21,35], M Sioli[15,16], C Sirignano[12], G Sirri[16], J S Song[32], M Spinetti[17], L Stanco[11], N Starkov[9], M Stipcevic[31], T Strauss[8,47], P Strolin[2,20], S Takahashi[27], M Tenti[15,16], F Terranova[17], I Tezuka[36], V Tioukov[2], P Tolun[3], A Trabelsi[10], T Tran[7], S Tufanli[3,46], P Vilain[38], M Vladimirov[9], L Votano[17], J L Vuilleumier[6], G Wilquet[28], B Wonsak[24], V Yakushev[1], C S Yoon[32], T Yoshioka[27], J Yoshida[27], Y Zaitsev[25], S Zemskova[18], A Zghiche[14] and R Zimmermann[24]**

[1] INR-Institute for Nuclear Research of the Russian Academy of Sciences, RUS-117312 Moscow, Russia
[2] INFN Sezione di Napoli, I-80125 Napoli, Italy
[3] METU-Middle East Technical University, TR-06531 Ankara, Turkey
[4] SINP MSU-Skobeltsyn Institute of Nuclear Physics of Moscow State University, RUS-119992 Moscow, Russia
[5] Kobe University, J-657-8501 Kobe, Japan
[6] Albert Einstein Center for Fundamental Physics, Laboratory for High Energy Physics (LHEP), University of Bern, CH-3012 Bern, Switzerland
[7] IPNL, Université Claude Bernard Lyon 1, CNRS/IN2P3, F-69622 Villeurbanne, France
[8] ETH Zurich, Institute for Particle Physics, CH-8093 Zurich, Switzerland
[9] LPI-Lebedev Physical Institute of the Russian Academy of Sciences, RUS-117924 Moscow, Russia
[10] Unité de Physique Nucléaire et des Hautes Energies (UPNHE), Tunis, Tunisia
[11] INFN Sezione di Padova, I-35131 Padova, Italy
[12] Dipartimento di Fisica dell'Università di Salerno and INFN, I-84084 Fisciano, Salerno, Italy
[13] Dipartimento di Fisica dell'Università di Padova, I-35131 Padova, Italy
[14] LAPP, Université de Savoie, CNRS/IN2P3, F-74941 Annecy-le-Vieux, France
[15] Dipartimento di Fisica dell'Università di Bologna, I-40127 Bologna, Italy
[16] INFN Sezione di Bologna, I-40127 Bologna, Italy
[17] INFN—Laboratori Nazionali di Frascati dell'INFN, I-00044 Frascati (Roma), Italy
[18] JINR-Joint Institute for Nuclear Research, RUS-141980 Dubna, Russia
[19] INFN—Laboratori Nazionali del Gran Sasso, I-67010 Assergi (L'Aquila), Italy
[20] Dipartimento di Scienze Fisiche dell'Università Federico II di Napoli, I-80125 Napoli, Italy
[21] INFN Sezione di Bari, I-70126 Bari, Italy
[22] Dipartimento di Fisica dell'Università dell'Aquila and INFN, I-67100 L'Aquila, Italy

[23] IPHC, Université de Strasbourg, CNRS/IN2P3, F-67037 Strasbourg, France
[24] Hamburg University, D-22761 Hamburg, Germany
[25] ITEP-Institute for Theoretical and Experimental Physics, RUS-117259 Moscow, Russia
[26] University of Münster, D-48149 Münster, Germany
[27] Nagoya University, J-464-8602 Nagoya, Japan
[28] Department of Physics, Technion, IL-32000 Haifa, Israel
[29] Università degli Studi di Urbino 'Carlo Bo', I-61029 Urbino, Italy
[30] Toho University, J-274-8510 Funabashi, Japan
[31] IRB-Rudjer Boskovic Institute, HR-10002 Zagreb, Croatia
[32] Gyeongsang National University, ROK-900 Gazwa-dong, Jinju 660-300, Korea
[33] Aichi University of Education, J-448-8542 Kariya (Aichi-Ken), Japan
[34] Dipartimento di Fisica dell'Università di Roma 'La Sapienza' and INFN, I-00185 Roma, Italy
[35] Dipartimento di Fisica dell'Università di Bari, I-70126 Bari, Italy
[36] Utsunomiya University, J-321-8505 Tochigi-Ken, Utsunomiya, Japan
[37] Fachbereich Physik der Universität Rostock, D-18051 Rostock, Germany
[38] IIHE, Université Libre de Bruxelles, B-1050 Brussels, Belgium
E-mail: bertolin@pd.infn.it, cecile.jollet@cern.ch and anselmo.meregaglia@cern.ch

*New Journal of Physics* **13** (2011) 053051 (22pp)
Received 10 February 2011
Published 26 May 2011
Online at http://www.njp.org/
doi:10.1088/1367-2630/13/5/053051

**Abstract.** The OPERA experiment is based on a hybrid technology combining electronic detectors (EDs) and nuclear emulsions. OPERA collected muon–neutrino interactions during the 2008 and 2009 physics runs of the CNGS neutrino beam, produced at CERN with an energy range of about 5–35 GeV. A total of $5.3 \times 10^{19}$ protons on target equivalent luminosity have been analysed with the OPERA EDs: scintillator strips target trackers and magnetic muon spectrometers equipped with resistive plate gas chambers and drift tubes, allowing a detailed reconstruction of muon–neutrino interactions.

[39] Author to whom any correspondence should be addressed.
[40] Now at INFN—Laboratori Nazionali del Gran Sasso, I-67010 Assergi (L'Aquila), Italy.
[41] Now at INAF/IASF, Sezione di Milano, I-20133 Milano, Italy.
[42] Now at Dipartimento di Fisica dell'Università di Roma 'La Sapienza' INFN, I-00185 Roma, Italy.
[43] Now at Pusan National University, Geumjeong-Gu Busan 609-735, Korea.
[44] Now at INFN—Laboratori Nazionali di Frascati dell'INFN, I-00044 Frascati (Roma), Italy.
[45] Now at Asan Medical Center, 388-1 Pungnap-2 Dong, Songpa-Gu, Seoul 138-736, Korea.
[46] Now at SUBATECH, CNRS/IN2P3, F-44307 Nantes, France.
[47] Now at Albert Einstein Center for Fundamental Physics, Laboratory for High Energy Physics (LHEP), University of Bern CH-3012 Bern, Switzerland.

Charged current (CC) and neutral current (NC) interactions are identified, using the measurements in the EDs, and the NC/CC ratio is computed. The momentum distribution and the charge of the muon tracks produced in CC interactions are analysed. Calorimetric measurements of the visible energy are performed for both the CC and NC samples. For CC events, the Bjorken-$y$ distribution and the hadronic shower profile are computed. The results are compared with a detailed Monte Carlo simulation of the response of EDs.

**Contents**



## 1. Introduction

OPERA [1] is a hybrid experiment based on electronic detectors (EDs) and nuclear emulsions. It is exposed to the long-baseline CNGS beam [2] from CERN to the Gran Sasso underground laboratory (LNGS) 730 km away from the neutrino source. The main purpose of the experiment is the observation of $\nu_\mu$ to $\nu_\tau$ oscillations in the direct appearance mode. The $\nu_\tau$ are identified through the measurement of the $\tau$ leptons produced in their charged current (CC) interactions. The neutrino runs started in 2008 and a first $\nu_\tau$ candidate has recently been observed [3]. The beam is mainly composed of $\nu_\mu$; interactions due to the $\bar{\nu}_\mu$, $\nu_e$ and $\bar{\nu}_e$ contaminations amount to 2.1%, 0.80 and 0.07% of the $\nu_\mu$ CC event rate. In the following sections, the $\nu_\mu$ interactions collected in the 2008 and 2009 runs, corresponding to $5.3 \times 10^{19}$ protons on target (p.o.t.), are analysed with fully operating EDs, which have taken data for more than 98% of the active beam time.

The EDs have many uses in the OPERA analysis flow in addition to their crucial role in the trigger, in the location of the interaction point in the target volume and in the muon identification

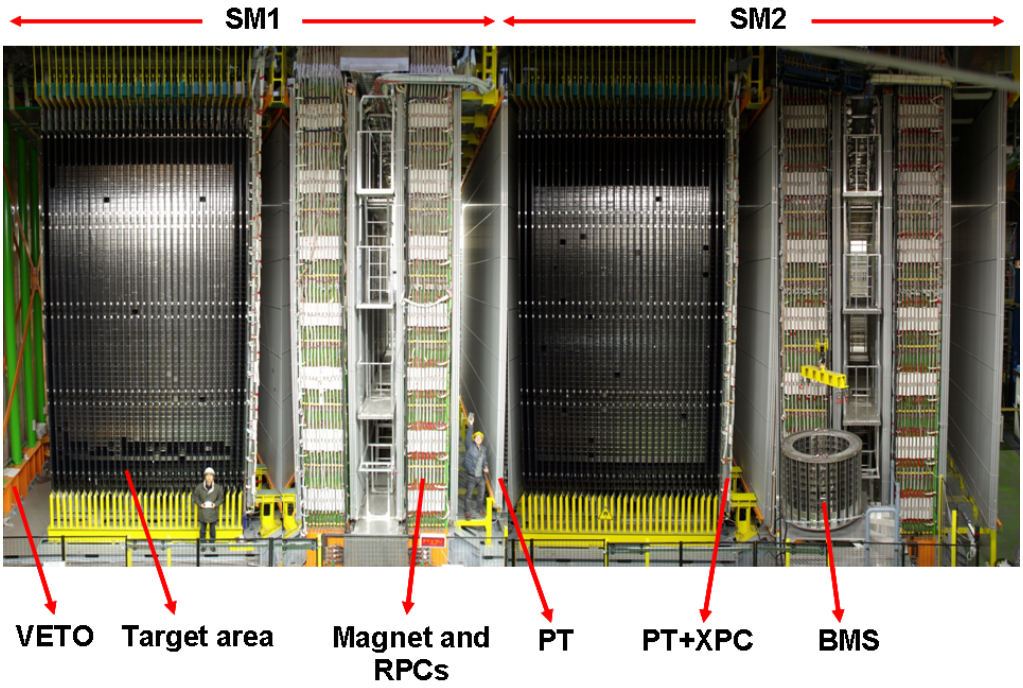


**Figure 1.** View of the OPERA detector; the neutrino beam enters from the left. The upper horizontal lines indicate the two identical super-modules (SM1 and SM2). The target area is made of walls filled with lead/emulsion bricks interleaved with 31 planes of plastic scintillators (TT) per SM. The VETO detector and a magnet with its inserted RPC planes are indicated by arrows, as well as some PT and XPC planes. The brick manipulator system (BMS) is also visible. See [4] for more details.

process. Thus, in this paper we discuss the OPERA ED performances in event selection, muon identification, momentum and charge reconstruction and calorimetry measurements.

The main features of the OPERA EDs are presented first, followed by a review of the Monte Carlo (MC) simulation and of the event reconstruction procedure. CC and neutral current (NC) interaction measurements are then discussed. The NC-to-CC ratio, the muon momentum spectrum, the reconstructed energy and the hadronic shower profile are investigated and a detailed comparison with an MC simulation is presented. This analysis is also a benchmark to establish the quality of the MC simulation related to the EDs.

## 2. OPERA electronic detectors (EDs)

As shown in figure 1, the OPERA detector [4] is composed of two identical super-modules (SMs). Each of them has a target section composed of target walls filled with lead/emulsion bricks alternated with walls of scintillator strips that constitute the target tracker (TT). Each target wall contains about 2920 bricks and only 53 walls out of 62 are filled. A brick is a mechanical unit that contains 57 emulsion films interleaved with fifty-six 1 mm thick lead plates. The transverse size of the brick is $12.8 \times 10.2\,\mathrm{cm}^2$. Each emulsion film has two 44 $\mu$m thick

emulsion layers deposited on a 205 $\mu$m thick plastic base. Each TT wall is composed of a pair of orthogonal scintillator strip arrays with an effective granularity of $2.6 \times 2.6\,\mathrm{cm}^2$ and has a surface of $6.7 \times 6.7\,\mathrm{m}^2$ transverse to the beam direction. Strips are read out via wavelength shifting (WLS) fibres connected to multi-anode photomultiplier tubes. The total masses of the lead/emulsion bricks and scintillator strips are about 1.25 and 0.9 kton, respectively.

A muon spectrometer at the end of each SM is used to identify muons and to measure their momentum and the sign of their charge. Each spectrometer consists of a dipolar magnet with two arms made of 12 iron plates; the measured magnetic field strength is 1.52 T. The two arms are interleaved with six vertical drift-tube planes, the precision trackers (PTs), for the precise measurement of the bending of the muon tracks. Planes of resistive plate chambers (RPCs) are inserted between the iron slabs of the magnets, 11 planes in each arm. Each RPC plane, $8.7 \times 7.9\,\mathrm{m}^2$ transverse to the beam direction, is equipped with two orthogonal sets of copper readout strips. These planes provide a coarse tracking, a range measurement of the stopping particles and a calorimetric analysis of the hadrons escaping the target along the incoming neutrino direction. Two planes of resistive plate chambers (XPC), with the readout strips tilted by $\pm 42.6^\circ$ with respect to the horizontal, are also placed after each target section to solve left/right ambiguities in the track pattern recognition. Together with the RPCs, the XPCs are used to provide an external trigger to the PTs. A $10 \times 9.12\,\mathrm{m}^2$ anti-coincidence glass RPC detector, the VETO, is placed in front of the first SM to exclude (or tag) interactions occurring in the material and in the rock upstream of the target. Although the EDs are not conceived to perform calorimetric measurements, they can be used for this purpose with a coarse resolution.

An example of a CC event as seen by the OPERA EDs is shown in the top part of figure 2, where the long tail of hits easily identifies a very high momentum muon track. The bottom part of figure 2 shows an NC event. The connection between the EDs and the nuclear emulsion data is described in [3, 5, 6].

## 3. Monte Carlo (MC) simulations

### *3.1. Event generation*

CC interactions can occur in the quasi-elastic (QE), resonant (RES) or deep inelastic scattering (DIS) regimes. In the QE and RES processes, the hadronic system observable in the detector is faint as most of the incoming neutrino energy is transferred to the final state lepton. Conversely, in the DIS process, a prominent hadronic system is observed in the detector. In order to obtain a prediction for the number of expected neutrino interactions in OPERA, the differential neutrino cross sections, $\mathrm{d}\sigma/\mathrm{d}E$, for the CC-DIS, CC-QE and CC-RES processes on an isoscalar target, known from other experiments [7], are convoluted with the CNGS neutrino flux. The mean energy of the incoming beam is 17.7 GeV [8] if the long tail extending above 100 GeV is not included. Only 0.6% of the total flux has an energy exceeding 100 GeV; this corresponds to less than 4% of the $\nu_\mu$ CC event rate on an isoscalar target [2]. Once the detector target mass and the number of recorded p.o.t. are defined, the absolute prediction for the expected number of interactions is computed together with the relative fractions of each process. The CC-DIS, CC-QE and CC-RES fractions are corrected for the non-isoscalarity of the materials used in the OPERA detector. The CC-DIS process is found to be dominant with a fraction exceeding 90%. Using the procedure outlined in [7], the NC-to-CC ratio on an isoscalar target is predicted to be 0.31, while it is 0.29 once the non-isoscalarity corrections are taken into account. Hence, the

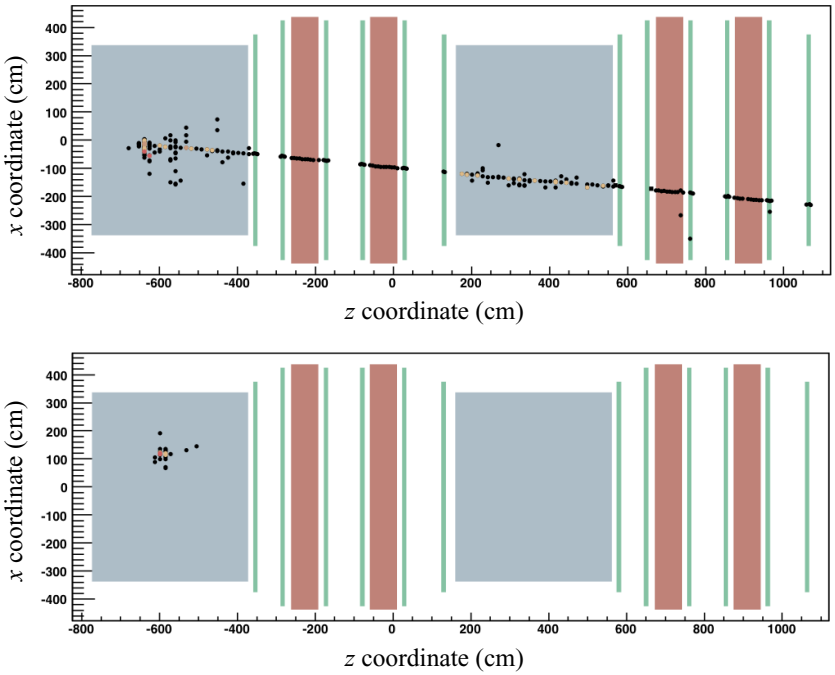


**Figure 2.** Examples of CC (top) and NC (bottom) events as seen in one projection view of the OPERA EDs. In this view, the two SMs can be recognized: for each of these, the target is followed by the muon spectrometer.

NC contribution is also fixed. Only NC interactions in the DIS regime are considered as final state particles have to be observed in the EDs. The final states for the different processes, CC-DIS, CC-QE, CC-RES and NC-DIS, are generated using NEG MC program [9], developed in the framework of the NOMAD experiment [10]. NEG MC is supplied with the CNGS neutrino spectrum up to 400 GeV. The generated events can then be mixed according to the appropriate fractions.

### *3.2. Environment simulation of the OPERA detector*

For the event simulation in the target, neutrino interaction primary vertexes are generated in the lead/emulsion volumes as well as in the volumes of the TT scintillator strips. The lead represents 93% of the target mass, the rest being emulsion films. Neutrino interactions occur not only in the target but also in other OPERA detector structures, such as spectrometers, in any material present in the experimental hall, including the BOREXINO [11] detector and its related facilities, and in the surrounding rock. The ratio between the number of recorded interactions occurring inside and outside the target is about 1–6. As a consequence, primary vertexes have been generated in all of the above-mentioned volumes, since final state particles from any of these volumes may easily reach the OPERA target. Owing to the asymmetric beam energy profile, with a tail at very high energy, a large enough volume of rock has to be considered. Upstream of the detector, a cylinder of rock, 35 m in radius and 300 m in length, has been used in the simulation. The rock volume surrounding the detector has the shape of a cylinder with a radius of 35 m and an inner empty volume corresponding to the LNGS Hall C shape hosting

**Table 1.** Efficiencies for the selection of contained events.

| Type | Contained fraction (%) |
|---|---|
| CC | $97.6 \pm 1.4$ |
| NC | $83.0 \pm 1.6$ |

the OPERA detector. MC studies show that 99% of the external events with hits reaching the OPERA detector are contained in a volume that is 35% smaller than the simulated one. Once primary vertexes are generated, the produced outgoing particles are propagated through the different simulated volumes and their interaction with matter, either with passive elements, such as the rock, or with a sensitive detector volume, is simulated using the GEANT3 [12] Virtual MC simulation package, version 1.10.

## 4. Event reconstruction

In order to provide a comparison with the data, a reconstruction of the simulated neutrino interactions is performed, using the same algorithms as for real data, and the efficiencies of the different analysis steps, such as the selection of neutrino interactions with the primary vertex contained in the target, NC versus CC event tagging or muon identification, are evaluated.

### *4.1. Selection of neutrino interaction events inside the target*

The OPERA DAQ system [4, 13] records with high efficiency all of the interactions leaving a significant activity in the OPERA detector. To achieve this, the ED data are actually acquired in triggerless mode since the readout of the front-end electronics is asynchronous with the data, time stamped with a 10 ns clock. A minimum bias filter is applied at the level of subdetectors in order to reduce the detector noise. The event building is then performed by collecting all of the hits in a sliding time window of 3000 ns and requiring hits in the $x$ and $y$ projections of at least two TT planes or a TT plane with the sum of the photomultiplier signals exceeding 1500 ADC counts, and the presence of at least 10 hits. If a muon track is present in the final state, the trigger efficiency of the DAQ system, estimated with MC methods, exceeds 99%. Even in the worst configuration where a $\nu_\mu$ to $\nu_\tau$ oscillation occurs followed by a QE $\nu_\tau$ interaction and a $\tau$ to $e$ decay, the trigger efficiency, averaged over the $\nu_\mu$ energy spectrum, exceeds 95%.

Cosmic-ray-induced events are also recorded [14] but they can be easily rejected as they are not in time with the CNGS beam. Therefore an almost pure sample of 31 576 interactions in time with the beam, with the primary vertex contained inside or outside the OPERA target, was obtained for the 2008–2009 neutrino runs. As events occurring in the target represent a small fraction of the total number of recorded events, an automatic algorithm, OpCarac [15], identifies such events, hereafter called 'contained' events. The contained events are more precisely those located in the target volume actually filled with bricks; this volume is fully instrumented by the TT, the walls of which are larger than the target walls. Events not fulfilling this requirement are hereafter called 'external' events. The OpCarac algorithm efficiency, estimated as the ratio between the number of MC events generated in the target volume and selected as contained to the total number of MC events generated, is high, as shown in table 1, in particular for CC events.

The external events are mostly due to CC interactions occurring in the rock surrounding the detector. The final state muon is crossing the full detector or entering from the sides. These events are easily identified and rejected by OpCarac. The presence of the VETO system is particularly helpful when the muon is entering the detector from the front. The number of recorded external events with this topology was compared to MC expectations. The data and MC are in agreement within the 10% error on the expected number of $\nu_\mu$ CC events due to the uncertainty on the total beam flux and on the $\nu_\mu$ CC cross section. Further MC studies show that CC events occurring in the rock surrounding the Hall C volume, in which the final state muon escapes detection, can also generate secondary particles produced at a large angle with respect to the incoming neutrino direction and hence reaching the target volume. In this case, the observed activity is mainly concentrated at the edges of the TT. These events appear as low activity NC events. Dedicated MC studies show that the spatial distribution of the low activity NC events measured in data and MC agree within the quoted 10% uncertainty. Due to the low activity in the EDs, these events are difficult to distinguish from genuine NC events occurring in the target. The contribution of NC interactions outside the target volume to the external event sample was checked through MC to be 20% of the overall external sample. In order to keep the efficiency for NC events occurring in the target high, a contamination of external events is unavoidable. While the CC sample is basically free of external events, the contamination of the NC sample is at the 10% level and 3% for the whole NC+CC sample.

### *4.2. Muon identification*

The muon identification performed by the EDs is of primary importance in the OPERA analysis flow because:

- The $\tau$ muonic decay is a 'golden channel' to tag the $\nu_\mu$ to $\nu_\tau$ oscillation since it is the only channel where the momentum and charge of the decay daughter can be measured.
- The identification of a muon track originating from the primary vertex is of crucial importance to discard all of the $\nu_\mu$ CC inclusive interactions, which are a source of background for the $\tau$ search.
- The muon charge measurement allows one to discriminate muons coming from $\tau$ decay, with negative charge, from those produced by the decays of charmed particles, with positive charge. This background is unfavourably large as charm is produced in $\sim 4\%$ of CC interactions and the charm branching ratio into $\mu^+$ is $\sim 18\%$ [7].

According to the requirements defined in the OPERA detector proposal, a CC tagging efficiency or similarly a muon identification efficiency greater than 95% has to be attained. Two algorithms have been developed [16]: the first one is based on global event topology and is therefore independent of the track reconstruction efficiency. It can be applied to all of the events; it is used for an evaluation of the NC/CC ratio, and it also provides a general veto for NC events. The second algorithm relies on the muon track reconstruction and it can therefore be applied only to events where a track exists; it is mandatory for the connection of the muon track between EDs and emulsions.

In the first algorithm, the criterion to classify CC and NC events is based on the total number of ED planes containing hits ($N_{\mathrm{ED}}$). For the TT subdetector, $N_{\mathrm{ED}}$ is obtained by counting the number of walls with signals in either of the two orthogonal planes; for the RPC subdetector the number of planes with signals in either of the two orthogonal sets of readout strips is

**Table 2.** MC efficiencies for CC and NC selection using the cut on $N_{ED}$. If $N_{ED} > 14$, the event is classified as CC, otherwise it is classified as NC.

| Type | Correctly identified fraction (%) |
|---|---|
| CC | $95.5 \pm 1.4$ |
| NC | $76.0 \pm 1.2$ |

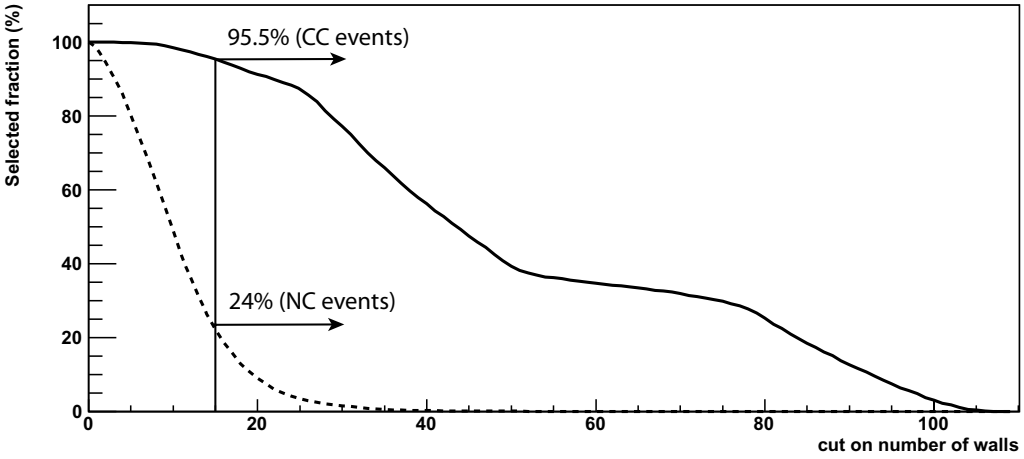


**Figure 3.** Integral fraction of selected events as a function of the cut on $N_{ED}$ for MC CC events (solid line) and MC NC events (dashed line). For this figure, the contained event requirement is not applied.

considered. The TT walls and the RPC planes are equally treated in this calculation. The energy lost by a minimum ionizing particle between two consecutive RPC planes is 57.1 MeV. Between two TT walls it is 71.4 MeV, 25% larger. The corresponding numbers of interaction lengths are, respectively, 0.298 and 0.328, 10% larger. The ratio between $dE/dx$ and the interaction length of the two media is not so large as to justify a different treatment in the algorithm applied. Furthermore, this difference is present in both the data and MC. In order to meet the requirement of the OPERA detector proposal of a CC tagging efficiency greater than 95%, the lower cut on $N_{ED}$ must be set to 14 planes, as can be seen in figure 3. Correspondingly, a large contamination of true NC events wrongly tagged as CC cannot be avoided. MC studies showed that starting from a pure sample of NC events, about 24% are erroneously tagged as CC, 6% relative to the full sample. Events with $N_{ED} \leqslant 14$ planes are instead tagged as NC. The tagging efficiencies are summarized in table 2. The $N_{ED}$ distributions for data and MC events are shown in figure 4; the agreement is reasonable.

The second algorithm is based on a precise reconstruction and identification of the muon track. The track reconstruction relies on a sequence of algorithms. Primarily the ED hits are connected to form tracks in both longitudinal projections by a pattern recognition algorithm. Then the three-dimensional (3D) tracks are reconstructed by associating tracks in the two projections. A Kalman filter [17] is also used to calculate the momentum and to reject hits wrongly assigned to tracks. The length times density is then computed and used to identify a generic track as a muon track. The length is defined by adding straight distances between

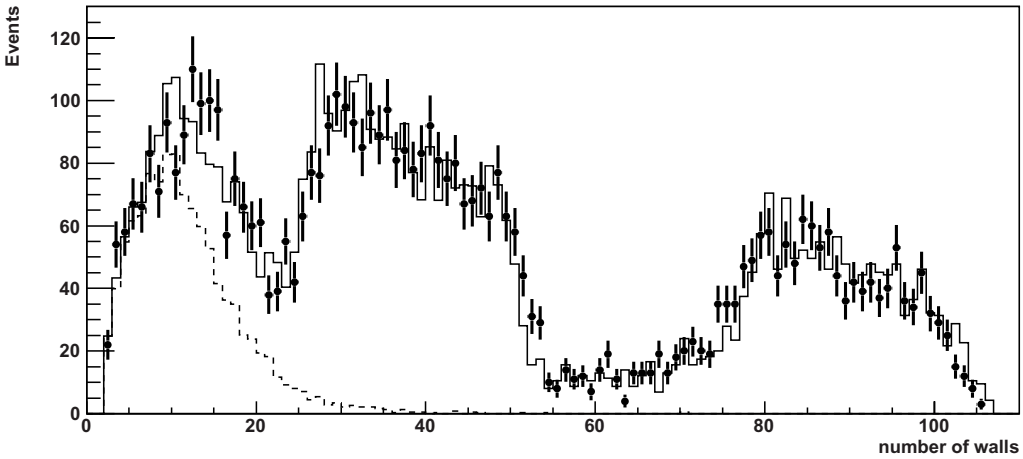


**Figure 4.** Number of hit walls for data (dots with error bars) and MC (solid line) contained events. The first bump is mainly due to NC events (dashed line), whereas the second and third ones originate from CC events crossing one and two SMs, respectively. The MC distribution has been normalized to data.

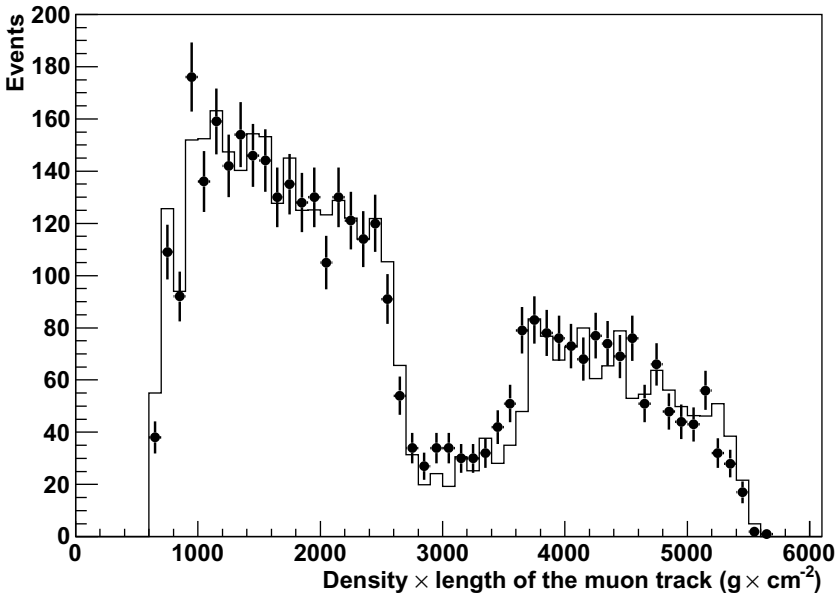


**Figure 5.** Length × density comparison for data (dots with error bars) and MC (solid line) for events classified as CC (i.e. length × density $> 660\,\mathrm{g\,cm^{-2}}$). The MC distribution has been normalized to data.

consecutive TT and/or RPC hits (TT walls are spaced apart by about 13 cm and RPC planes by about 7 cm) along the whole track length. The actual detector structure along the track path fixes the value to be used for density. The muon identification criterion is based on a cut on the length times density of the longest reconstructed 3D track in the event. Requiring a muon identification at the level of 95% implies a cut at $660\,\mathrm{g\,cm^{-2}}$. The length times density distributions for data and MC, above the selection cut, are shown in figure 5, where the MC distribution has been

normalized to the data. The MC simulation reproduces the data trend well. For each track identified as a muon by the length times density criterion, the algorithm provides an estimate of the momentum. If the track stops in the target or leaves the target but does not fully cross at least one spectrometer arm, the energy is measured by range and the charge measurement is not available. MC studies show that the NC contamination of the sample of events with at least one muon track is 5.2%. In the sample of events where a spectrometer is crossed, the NC contamination is as small as 0.8%. In addition, if at least one muon with negative charge is required, the contamination drops to 0.4%.

### *4.3. NC-to-CC ratio*

In this study, the algorithm based on the number of ED planes with hits is used for identifying muons and hence CC events. Applying first the contained event selection algorithm and then the muon selection criterion on $N_{\mathrm{ED}}$ to the data, 4332 events are classified as CC ($81.4 \pm 2.8\%$) and 989 events as NC ($18.6 \pm 0.7\%$). This gives an NC-to-CC ratio of $0.228 \pm 0.008$.

The MC estimation of the NC-to-CC ratio has to take into account the efficiencies of both the contained events selection (see table 1) and the correct CC and NC event tagging (see table 2). Moreover, as already seen in section 4.1, detailed studies of the event selection show that in the data there is a non-negligible contamination of external events. Scaled to the number of true CC events occurring inside the target, this contamination was estimated to be 2.96% for the NC and 0.78% for the CC samples. The number of reconstructed CC and NC events can be estimated via the following equations,

$$\begin{aligned} \mathrm{CC}_{\mathrm{rec}} &= \epsilon^{\mathrm{C}}_{\mathrm{CC}} \times \epsilon_{\mathrm{CC}} \times n_{\mathrm{CC}} + \epsilon^{\mathrm{C}}_{\mathrm{NC}} \times (1 - \epsilon_{\mathrm{NC}}) \times R_{\mathrm{NC/CC}} \times n_{\mathrm{CC}} + 0.0078 \times n_{\mathrm{CC}}, \\ \mathrm{NC}_{\mathrm{rec}} &= \epsilon^{\mathrm{C}}_{\mathrm{CC}} \times (1 - \epsilon_{\mathrm{CC}}) \times n_{\mathrm{CC}} + \epsilon^{\mathrm{C}}_{\mathrm{NC}} \times \epsilon_{\mathrm{NC}} \times R_{\mathrm{NC/CC}} \times n_{\mathrm{CC}} + 0.0296 \times n_{\mathrm{CC}}, \end{aligned} \tag{1}$$

where

- $\epsilon^{\mathrm{C}}_{\mathrm{CC}}$ is the efficiency of the contained events selection algorithm for the CC MC sample.
- $\epsilon^{\mathrm{C}}_{\mathrm{NC}}$ is the efficiency of the contained events selection algorithm for the NC MC sample.
- $\epsilon_{\mathrm{CC}}$ is the efficiency of the CC selection algorithm for the CC MC sample.
- $\epsilon_{\mathrm{NC}}$ is the efficiency of the NC selection algorithm for the NC MC sample.
- $n_{\mathrm{CC}}$ is the true number of CC MC events.
- $R_{\mathrm{NC/CC}}$ is the true NC/CC ratio.

Using the value of $R_{\mathrm{NC/CC}}$ computed in section 3.1, 0.29, and those of the efficiencies given in tables 1 and 2, the MC expectation for the NC-to-CC ratio comes to 0.257.

The efficiencies for the contained events selection and for the NC and CC tagging are extracted from the MC simulation, each with a statistical uncertainty in the range of 1–2%, as shown in tables 1 and 2. These errors are then numerically propagated in equation (1) to obtain a statistical uncertainty of 0.018 on the MC NC-to-CC ratio.

Systematic uncertainties due to CC and NC event tagging can be estimated by changing the cut on $N_{\mathrm{ED}}$. Varying the cut from 10 to 25 planes, the maximum discrepancy between data and MC in the NC-to-CC ratio is $\pm 0.019$. Another source of systematics comes from the uncertainties in the contained events selection algorithm. As can be seen in table 1, 17% of the NC MC events are not selected. Out of these, 4.2% are discarded since they would not fulfil

**Table 3.** NC/CC ratio for data and MC.

| | NC/CC |
|---|---|
| Data | $0.228 \pm 0.008$ |
| MC | $0.257 \pm 0.031$ |

the trigger condition (see section 4.1). The remaining 12.8% of the events are in a transition region, with little activity recorded in the detector. Conservatively, a 50% error is assumed for this particular topology of NC events. The same computation for the CC events gives about a 1% error. This propagates into an error of $\pm 0.015$ on the final result. In order to check for additional systematic uncertainties due to the contained event selection algorithm, data and MC calculations for the NC-to-CC ratio are repeated using events with the primary vertex in the first and the second SM separately. No difference is found in either the simulation or the real data where the values obtained for the ratio agree within 1 sigma. Therefore, a possible contribution to the systematic error of the measurement is negligible.

The last source of uncertainties is on the number of external events that affect mostly the NC sample. This uncertainty is obtained by inspecting the agreement between data and MC in variables that are particularly sensitive to the external background component, such as the visible energy and the 3D position of the events. While genuine NC events are uniformly distributed inside the target, external events tend to be more concentrated towards the edges. This analysis showed that the expected number of background events in data and MC are in reasonable agreement, within an uncertainty safely estimated to be in the range of $-15$ to $+24\%$. After numerical propagation in equation (1), this translates into an error of $\pm 0.006$ in the final result. Adding the different contributions in quadrature, the overall systematic uncertainty on the NC-to-CC ratio for the MC is $\pm 0.025$.

The results are shown in table 3, where statistical and systematic errors for MC have been added quadratically.

## 5. OPERA ED performances on neutrino event reconstruction

In the following paragraphs, data MC comparisons are presented for several reconstructed quantities characterizing neutrino interaction events.

### *5.1. Muon momentum reconstruction*

A first step in establishing the quality of the muon momentum reconstruction can be taken by comparing the momentum distribution measured in data and MC for the contained events. For this test, it is desirable to use a sample with a reduced NC contamination in order to disentangle the true muon reconstruction from possible effects due to background hadron tracks. Therefore, all events are required to have their muon momentum measured from the bending in the spectrometer. In addition, a negative measured charge is required. The measured muon momentum distribution is shown in figure 6 and compared to MC expectations. The MC has been normalized to the number of p.o.t. corresponding to the 2008–2009 data sample. The error in the MC prediction is obtained after taking into account the uncertainty in the value of the

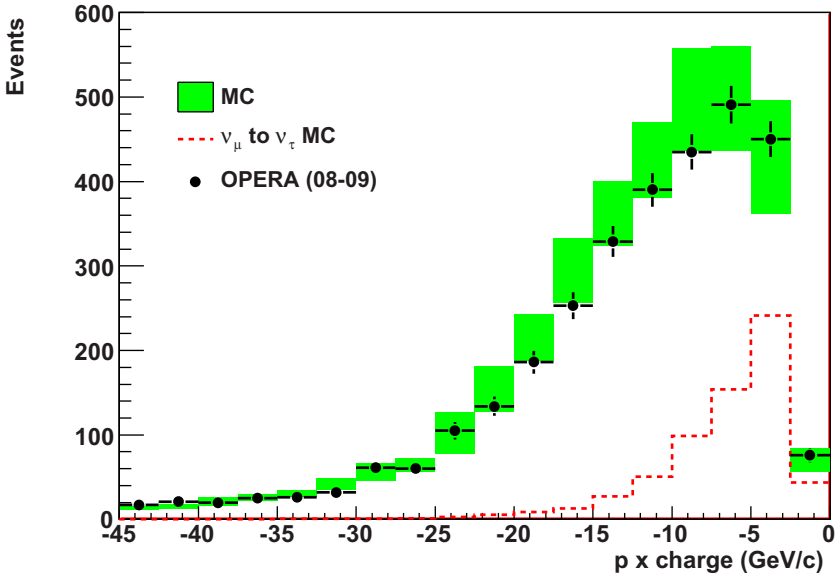


**Figure 6.** Muon momentum comparison (momentum × charge). Data are shown by dots; errors are statistical only. The MC prediction, normalized to the number of p.o.t. corresponding to the 2008–2009 data sample, is shown by the coloured area. The dominant source of the spread of the MC prediction is due to the 10% uncertainty on the expected number of $\nu_\mu$ CC events. For illustration purposes only, the lower dashed curve represents the contribution obtained from the $\nu_\mu$ to $\nu_\tau$ MC events with subsequent decay into $\mu$ of the final state $\tau$ lepton. The normalization of this contribution is arbitrary.

magnetic field, which translates into a 3% shift of the MC spectrum, and the already quoted 10% uncertainty on the expected number of $\nu_\mu$ CC events, the latter being the dominant source of uncertainty. The contribution obtained from the $\nu_\mu$ to $\nu_\tau$ MC events with subsequent decay into $\mu$ of the final state $\tau$ lepton is also shown in figure 6, with an arbitrary normalization, to show the interesting momentum region. The spectrum of $\mu$ from $\tau$ decay is much softer than the spectrum measured for $\nu_\mu$ CC interactions: the mean values obtained from the MC simulation are $-6.8$ and $-12.7\,\mathrm{GeV\,c^{-1}}$, respectively. In order to perform a shape comparison both, data and MC distributions have been normalized to 1. A $\chi^2$ value of 16.56 for 17 d.o.f. is obtained without considering the magnetic field and the incoming neutrino flux uncertainties. The overall normalization was also checked: the number of events in data and MC agree within 6%, well within uncertainties.

### *5.2. Muon charge reconstruction*

As mentioned in section 1, a $\bar{\nu}_\mu$ component is present in the beam, leading via the CC process to positive muon tracks. These can be used to test the muon charge reconstruction algorithm by performing a measurement of the $\mu^+$ to $\mu^-$ events ratio. The efficiency of the algorithm has been studied using CC MC events. It is defined as the fraction of simulated muon tracks reconstructed with the true charge. As expected, the charge determination uncertainty increases with the muon momentum. If an upper limit on the absolute value of the momentum is set

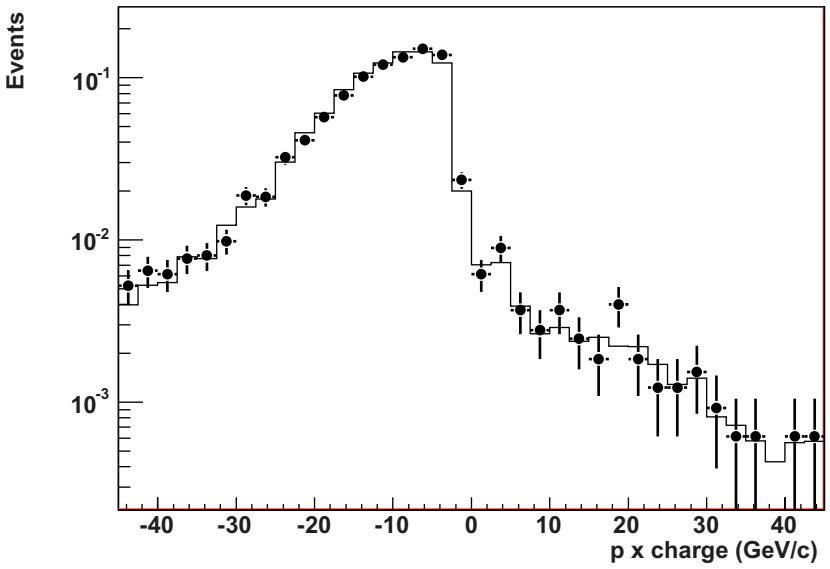


**Figure 7.** Muon charge comparison (momentum × charge): data (black dots with error bars) and MC (solid line) are normalized to one.

at 45 GeV c$^{-1}$, the wrong determination of the muon charge is smaller than 2%. The charge reconstruction efficiency is also reduced at low momentum. In this case, the 3D track identified as a muon may be a charged hadron and hence the measured charge is not that of the muon. This was not observed in MC events with the final state including a muon and negligible hadronic activity, as a confirmation of this hypothesis. Once again, if a lower limit on the absolute value of the momentum is set at 2.5 GeV c$^{-1}$, the wrong determination of the muon charge is smaller than 2%. For muon momenta between 2.5 and 45 GeV c$^{-1}$, the fraction of events with wrong charge determination is 1.2%. The $\mu^+$ to $\mu^-$ events ratio, within the selected momentum range, obtained from data can be directly compared with predictions based on the full MC sample: $3.92 \pm 0.37$ (stat.)% for data, and $3.63 \pm 0.13$ (stat.)% for MC. Figure 7 shows the momentum times charge distribution for data and MC, both normalized to one: the $\chi^2$ value is 23.34 for 35 d.o.f.

### *5.3. Energy reconstruction*

This section studies the energy reconstructed using the TT subdetector. A signal is measured at each end of the scintillator strips in terms of ADC counts (see [18] for details), and then converted into a number of photo-electrons (p.e.) according to the gain of the photomultiplier (PMT) channel. The sum of the number of p.e. measured on both sides is converted into an energy deposit (in MeV), according to the position of the hit along the strip and to a calibration curve that accounts for the attenuation of the signal along the strip fibre. This calibration has been performed using radioactive sources before detector assembly and cosmic ray data. First, the dependence of the number of p.e. of a minimum ionizing particle (mip) on the crossing position along the strip has been validated (see section 5.3.1) and used to compute the visible energy. Then a calibration of the EDs has been performed in order to convert the visible energy into total energy (see section 5.3.2). The reconstruction algorithms are used to study, in data and MC, the distributions of the Bjorken-$y$ variable (section 5.3.3).

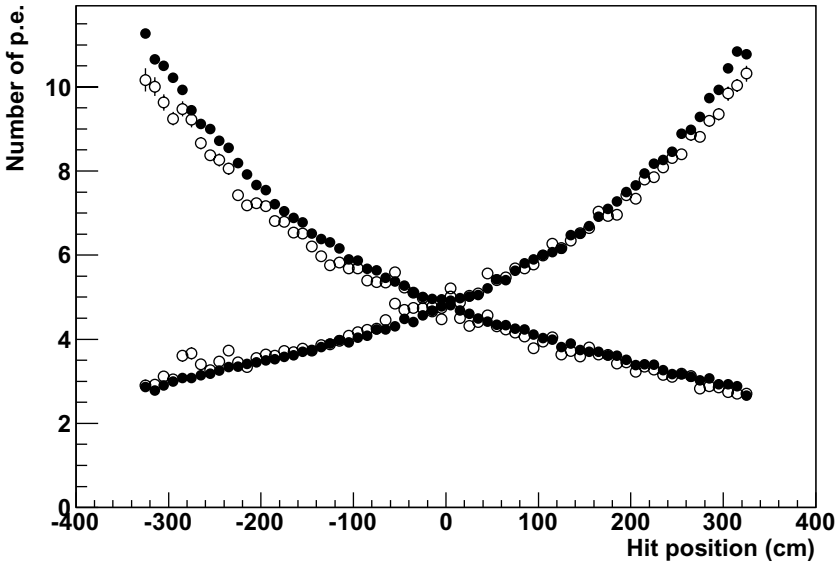


**Figure 8.** The number of detected p.e. on each extremity of the TT strips as a function of the hit position with respect to the left and right PMTs. The full circles are data and the empty ones are MC expectations.

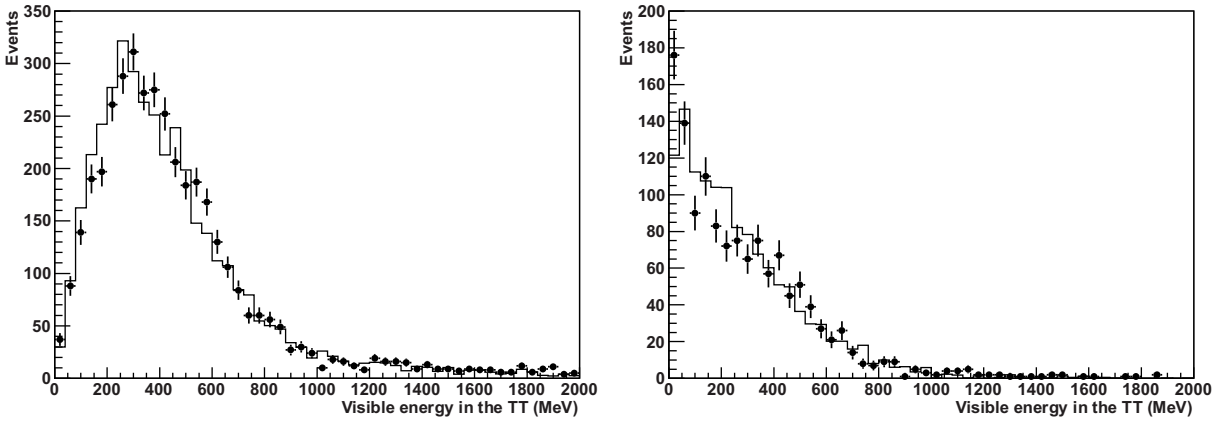


**Figure 9.** Energy deposit in the TT for events with at least one reconstructed muon (left) and events with no muon (right). Dots with error bars correspond to data and solid lines to MC. MC distributions are normalized to data.

*5.3.1. Visible energy.* Events with long tracks left by a mip have been selected and hits associated only with those tracks have been considered. In figure 8, the number of p.e. recorded on each side of the fibre is plotted as a function of the distance to the hit. A double exponential decrease fits both the data and MC. The number of p.e. recorded at the centre of the fibre is typically 5. The maximal discrepancy between data and MC is within 10%. The reverse relation is used for converting a number of p.e. into visible energy once the hit position is reconstructed. This has been done for events with at least one muon identified and events without muon identified separately; the comparison between data and MC is shown in figure 9. There is, on average, reasonable agreement between data and MC simulation; however, some discrepancies

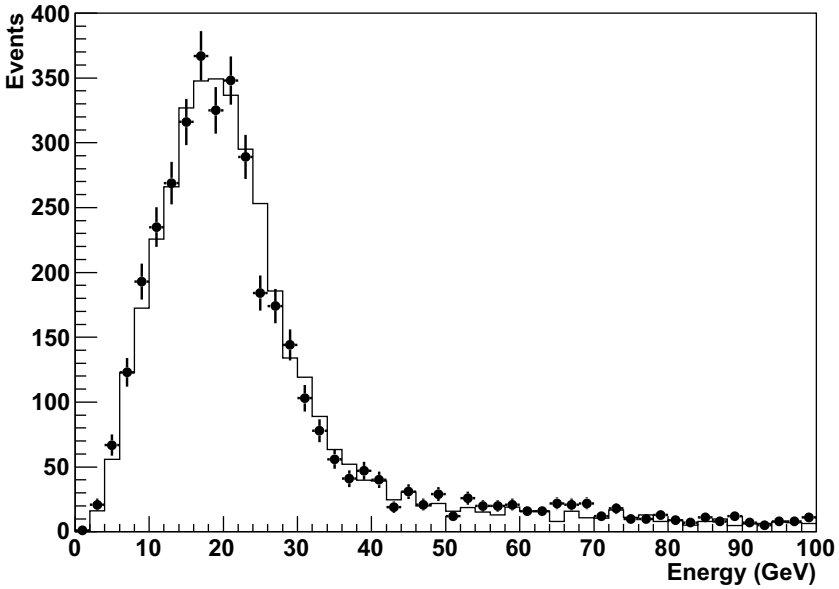


**Figure 10.** Total reconstructed energy for events with at least one identified muon for data (dots with error bars) and MC (solid line). The MC distribution is normalized to data.

can be seen at very low energy for NC events. The energy deposit for NC events has been studied discarding soft NC-like events; when there is at least one 3D reconstructed track in the event the low-energy disagreement disappears.

*5.3.2. Reconstructed energy.* In order to reconstruct the kinematical variables of an interaction, knowledge of the total hadronic energy is required. Based on an MC simulation, the relation between the true hadronic energy and the visible energy deposited in the TT and the RPC strips has been parameterized. The reverse parameterization is used to estimate the hadronic energy from the ED data. Details of the energy resolution can be found in appendix A.3. The results obtained by adding the hadronic and the muon energy are shown in figure 10 for events with at least one identified muon; the data and MC are in reasonable agreement.

*5.3.3. Bjorken-y.* The Bjorken-$y$ variable represents the fraction of the hadronic energy with respect to the incoming neutrino energy. For CC interactions,

$$\nu_\mu(k)N(P) \rightarrow \mu(k')X, \tag{2}$$

where $k$, $P$ and $k'$ are the quadrimomenta of the particles involved, and the Bjorken-$y$ variable is defined as

$$y = \frac{P \cdot (k - k')}{P \cdot k}. \tag{3}$$

In the laboratory frame, the Bjorken-$y$ variable can be computed as

$$y = 1 - \frac{E_\mu}{E_{\nu_\mu}} = \frac{E_{\text{had}}}{E_\mu + E_{\text{had}}}, \tag{4}$$

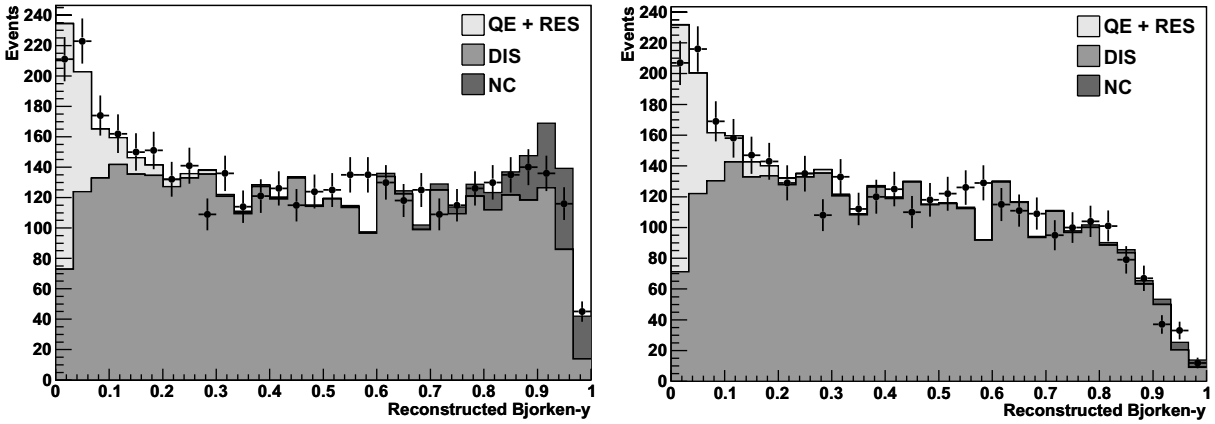


**Figure 11.** Bjorken-$y$ variable reconstructed in data (dots with error bars) and MC (shaded areas). The MC distributions are normalized to data. The different contributions of the MC are shown in different colours: QE + RES contribution in light grey, DIS contribution in grey and the NC contamination in dark grey. On the left, all of the events with at least one muon are shown, whereas on the right, the events for which the momentum is measured in the spectrometer are shown.

where $E_{\nu_\mu}$ is the incoming neutrino energy, $E_\mu$ the energy of the outgoing muon and $E_{\text{had}}$ the hadronic energy. Bjorken-$y$ connects the muon momentum measurement, performed in the spectrometer or by range, with the calorimetric measurements of all of the hadrons. The results for the events selected with at least a muon track and for the events with the muon momentum measured by the spectrometer are shown in figure 11 in the left and right plots, respectively. The agreement between data and MC simulation is reasonable: the $\chi^2$ values are 55.4 and 48.7, respectively, for 29 d.o.f. The sum of the QE and RES processes can be clearly seen as a peak at low $y$ values. The NC contribution shows up at values of Bjorken-$y$ close to one. Figure 11 shows that the NC contribution becomes negligible when a track with its momentum measured by the spectrometer is required. This analysis results in an overall cross check of the performances of the EDs.

### *5.4. Hadronic shower profile*

A precise implementation in the MC simulation of the hadronic activity observed in the data is very difficult; tools such as GHEISHA [19] and FLUKA [20] describe imperfectly the measurements available. Nevertheless, the hadronic activity is used, at least indirectly, in algorithms such as the contained events selection or the brick finding. Therefore, the hadronic shower profile in a sample of CC contained events has been analysed. The selected variables are the rms of the distribution of the shower profile in the $X$ and $Y$ projections (the transverse projections), where the TT hit positions are weighted by the number of collected p.e. The results are shown in figure 12 (left). Similarly, the longitudinal profile of the shower is shown in figure 12 (right). In order to correctly calculate the longitudinal profile, the muon track has been removed, relying on an algorithm that finds the point where the muon exits from the shower and a clear track shows up. Comparing the transverse profile, the hadronic activity measured in the

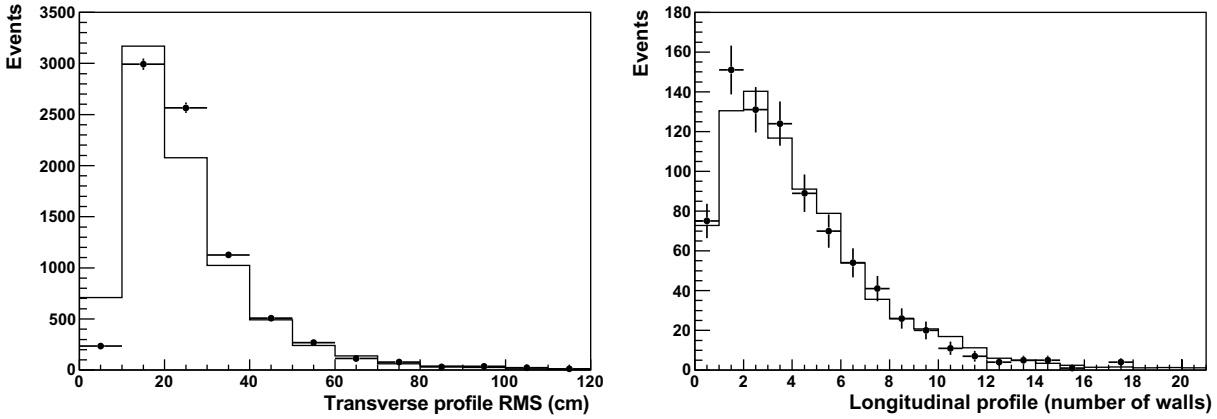


**Figure 12.** Transverse hadronic shower profile (left), in the $X$ and $Y$ projections, and longitudinal profile (right), in the number of TT walls. Data are shown by dots with error bars and MC by the solid line. MC distributions are normalized to data.

data is broader than that in MC, whereas this effect is not visible in the longitudinal profile of the shower. The simulation results shown here have been obtained with the GFLUKA option turned on in the GEANT3 simulation. The same comparison using the GHEISHA option yields a larger disagreement between data and MC.

## 6. Conclusions

The $\nu_\mu$ interaction data collected by the OPERA experiment in its two first running years, 2008 and 2009, have been analysed using the full potentialities of the EDs. During this period, all EDs were fully operational for more than 98% of the active beam time.

Neutral and charged current interaction events have been analysed, and a preliminary neutral to CC event ratio has been measured and found to be consistent with MC expectations. An analysis of the released energy profiles for both neutral and charged current events has been performed and good agreement was found between the data and MC.

CC events have been analysed in terms of muon momentum and charge reconstruction. In particular, the muon charge ratio has been found to be consistent with the expected $\bar{\nu}_\mu$ beam contamination.

In addition, CC events have been used to measure the total reconstructed energy and the Bjorken-$y$ distribution. Finally, the hadronic shower profile has been analysed and compared to an MC simulation. Although some characteristics of the energy profile are not reproduced in detail, the general description is satisfactory. The results presented have shown the excellent performances of the OPERA EDs and have provided a good understanding of their simulation and response.

## Acknowledgments

We thank CERN for commissioning the CNGS facility and for its successful operation; and we thank INFN for continuous support of the experiment during the construction, installation

**Table A.1.** Efficiency of the ED single strip or drift tube implemented in the MC simulation.

| Detector | Efficiency (%) |
|---|---|
| TT | 99 (threshold at 1/3 p.e.) |
| RPC | 95 |
| PT | 99 |

and commissioning phases through its LNGS laboratory. We acknowledge funding from our national agencies: Fonds de la Recherche Scientifique—FNRS and Institut Interuniversitaire des Sciences Nucléaires for Belgium, MoSES of Croatia, CNRS and IN2P3 of France, BMBF of Germany, INFN of Italy, JSPS (Japan Society for the Promotion of Science), MEXT (Ministry of Education, Culture, Sports, Science and Technology), QFPU (Global COE program of Nagoya University, 'Quest for Fundamental Principles in the Universe' supported by JSPS and MEXT) and Promotion and Mutual Aid Corporation for Private Schools of Japan, SNF, the Canton of Bern and the ETH Zurich of Switzerland, the Russian Federal Property Fund, grant 09-02-00300_a, 08-02-91005-CERN, the programs of the Presidium of the Russian Academy of Sciences 'Neutrino Physics' and 'Experimental and theoretical researches of fundamental interactions connected with work on the accelerator of CERN', programs for the support of leading schools of thought (grant no. 3517.2010.2), Federal Agency on Science and Innovations state contract 02.740.11.5092 of Russia, Department of Priority Directions of Science and Technologies, and a Korea Research Foundation grant (KRF-2008-313-C00201) of Korea. We are also indebted to INFN for fellowships and grants to non-Italian researchers. We thank the IN2P3 Computing Centre (CC-IN2P3) for providing computing resources for the analysis and for hosting the central database of the OPERA experiment. We are indebted to our technical collaborators for the excellent quality of their work over many years of design, prototyping and construction of the detector and its facilities. Finally, we thank our industrial partners.

## Appendix. A Simulation of the EDs

In this appendix, the simulation of the most relevant subdetectors, TT, RPC and PT, will be reviewed in some detail. The single strip, TT/RPC, or drift tube, PT, efficiencies implemented in the MC simulation are given in table A.1. The last subsection will also show the performances, in terms of energy resolution, of the calorimetric measurements that can be achieved with OPERA.

### *A.1. Simulation of the resistive plate chambers (RPCs)*

When a particle is tracked through the volume occupied by the RPC planes, one or more adjacent hit strips are created and the corresponding times are recorded. Nine planes in each SM are also used to generate a fast trigger signal used as an external trigger by the drift tubes of the PTs. This trigger signal is also accurately computed in the simulation. Due to the different widths of the horizontal and vertical sets of readout strips, a slightly different efficiency is implemented in the MC simulation. The efficiency in the MC is tuned from the observed multiplicity of vertical and horizontal strips measured for neutrino-induced muon tracks. From these data and from

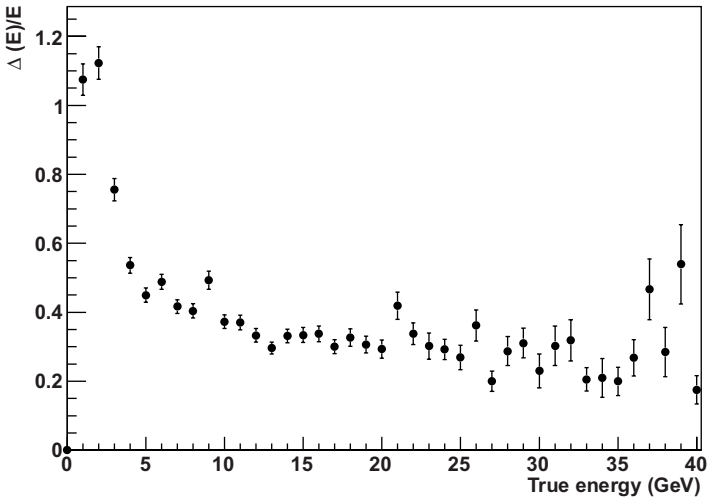


**Figure A.1.** MC energy resolution computed using the CNGS neutrino energy spectrum.

cosmic ray data, the average strip efficiency measured *in situ* exceeds 95%. The stability of the performances is monitored using cosmic ray data.

### *A.2. Simulation of the precision trackers (PTs)*

If a charged particle passes through the gas-filled volume of a PT drift tube, the hits in this volume are recorded, as well as the corresponding time. The hit closest to the sense wire is taken to determine the drift time using a drift time to distance relation. In addition, the drift time is smeared using a resolution function. The time information of the RPC hits in planes contributing to the trigger is used to generate a trigger time. The signal propagation delays in all corresponding cables and in the RPC strips are taken into account for a realistic simulation of the trigger time delay. The resulting trigger time is then subtracted from the time of the drift tube hit and this difference is used as an offset for the drift time. Thus trigger effects and the time of flight between the trigger planes and the drift tubes are properly accounted for. Also, the signal propagation delay on the drift tube wires and the signal cables is taken into account. In the simulation, the single tube efficiency is set to 99%. If no trigger is generated in an SM, no drift tube data are saved for this SM. The time to distance relation, the resolution function and the single tube efficiency have been determined using a test setup outside the LNGS, with the same operational parameters as those used onsite. Detector alignment is performed during dedicated cosmic ray runs without magnetic field. *In situ*, performances are monitored using cosmic ray data.

### *A.3. Simulation of the target tracker (TT)*

When a particle is tracked through the volume occupied by a TT scintillator strip, the energy deposited and the time are recorded. A corresponding light signal is generated, and the attenuation and the delay in the propagation through the strip via the WLS fibre up to the corresponding photomultiplier channel are computed. The signal is converted into a number of p.e. With the chosen threshold (1/3 of p.e.), the mean detection efficiency for a minimum

ionizing particle crossing the strip in the middle is higher than 99%. To make the detector description as realistic as possible, the crosstalk has also been included, i.e. the possibility that the signal deposited in one TT strip is recorded on a neighbouring photomultiplier channel. Calibrations are periodically performed and efficiencies, obtained from neutrino interaction data or cosmic ray data, are compared with the MC simulation. Using MC data, it is then possible to correlate the visible energy in the TT with the incoming neutrino energy. In the presence of an energy leakage from the TT into the spectrometer, the RPC data are also explicitly taken into account by the algorithm. The energy resolution reached is shown in figure A.1.

## References


[1] Guler M *et al* (OPERA Collaboration) 2000 CERN-SPSC-2000-028
[2] Elsener E K 1998 CERN 98-02, INFN/AE-98/05, CNGS project, http://proj-cngs.web.cern.ch/proj-cngs/
[3] Agafonova N *et al* (OPERA Collaboration) 2010 *Phys. Lett.* B **691** 138
[4] Acquafredda R *et al* (OPERA Collaboration) 2009 *J. Instrum.* **4** P04018
[5] Acquafredda R *et al* (OPERA Collaboration) 2006 *New. J. Phys.* **8** 303
[6] Anokhina A *et al* (OPERA Collaboration) 2008 *J. Instrum.* **3** P07005
[7] Nakamura K *et al* 2010 *J. Phys. G: Nucl. Part. Phys.* **37** 075021
[8] Ball A E *et al* (CERN—SL DIVISION) 2000 SL-Note-2000-063 EA
[9] Autiero D 2005 *Nucl. Phys. Proc. Suppl.* **139** 253
[10] Altegoer J *et al* (NOMAD Collaboration) 1998 *Nucl. Instrum. Methods* A **404** 96
[11] Alimonti G *et al* (BOREXINO Collaboration) 2002 *Astropart. Phys.* **16** 205
[12] Brun R *et al* 1987 *Technical Report* CERN-DD/EE/84-1, http://wwwasd.web.cern.ch/wwwasd/geant/
[13] Marteau J (OPERA Collaboration) 2010 *Nucl. Instrum. Methods* A **617** 291
[14] Agafonova N *et al* (OPERA Collaboration) 2010 *Eur. Phys. J.* C **67** 25–37
[15] Bertolin A and Tran N T 2009 *OPERA Public Note* 100
[16] Jollet C and Meregaglia A 2009 *OPERA Public Note* 101
[17] Fruhwirth R 1987 *Nucl. Instrum. Methods* A **262** 444
Billoir P 1984 *Nucl. Instrum. Methods* A **225** 352
[18] Adam T *et al* 2007 *Nucl. Instrum. Methods* A **577** 523
[19] Fesefeldt H C 1985 *Technical Report* PITHA 85-02
[20] Battistoni G *et al* 2007 *AIP Conf. Proc.* **896** 31–49